(1)

REPORT DOCUMENTATION PAGE

Form Approved
OMB No. 0704-0188

1. AGENCY USE ONLY (Leave blank)	2. REPORT DATE	3. REPORT TYPE AND DATES COVERED
	Oct 29, 1982	Final (4 May 82-31 Oct 1982

4. TITLE AND SUBTITLE

PLASMA ACCELERATOR AND ENERGY CONVERSION RESEARCH

5. FUNDING NUMBERS

61102F
2308/A1

AUTHOR(S)

Eugene V. Pawlik

PERFORMING ORGANIZATION NAME(S) AND ADDRESS(ES)

Jet Propulsion Laboratory
California Institute of Technology
Pasadena, CA 91109

8. PERFORMING ORGANIZATION REPORT NUMBER

AFOSR-TR- 89-1599

SPONSORING/MONITORING AGENCY NAME(S) AND ADDRESS(ES)

AFOSR
BLDG 410
BAFB DC 20332-6448

10. SPONSORING/MONITORING AGENCY REPORT NUMBER

AFOSR-ISSA-82-00044

11. SUPPLEMENTARY NOTES

12a. DISTRIBUTION/AVAILABILITY STATEMENT

Approved for public release;
distribution unlimited.

12b. DISTRIBUTION CODE

13. ABSTRACT (Maximum 200 words)

14. SUBJECT TERMS

15. NUMBER OF PAGES

41

16. PRICE CODE

17. SECURITY CLASSIFICATION OF REPORT	18. SECURITY CLASSIFICATION OF THIS PAGE	19. SECURITY CLASSIFICATION OF ABSTRACT	20. LIMITATION OF ABSTRACT
unclassified	unclassified		

NSN 7540-01-280-5500

Standard Form 298 (890104 Draft)
Prescribed by ANSI Std. 239-18
298-01

AFOSR-TR- 82-1599

FINAL REPORT ON

PLASMA ACCELERATOR AND ENERGY CONVERSION RESEARCH

TO

U.S. Air Force Office of Scientific Research

JPL Proposal No. 80-1849

AUTHOR - EUGENE V PAWLIK

Grant # - AFOSR-ISSA-82-00044

TABLE OF CONTENTS

AMTEC ELECTRODE RESEARCH

Report for the period July 1, 1982 through October 29, 1982.

STATEMENT OF WORK:

The tasks to be performed in the AMTEC research were as follows:

1. To construct by magnetron sputter deposition three AMTEC porous electrodes of 1-3 μm thickness, one of LaB_6 on a β''-alumina solid electrolyte tube, and two of molybdenum-titanium alloy, one of which shall be in the range of 0.2% - 0.5% titanium and the other in the range of 0.5% - 5% titanium.

2. To characterize the morphology and composition of the deposited electrodes before and after high temperature operation and sodium electrolysis by scanning electron microscopy and ion microprobe chemical analysis.

3. To investigate the electrochemical performance and measure sodium vapor transport properties of the deposited electrodes by determining current-voltage characteristics and by current interrupt measurements. A current interrupt test circuit was to be designed and assembled for this purpose.

4. To analyze electrode performance in terms of chemical and morphological characteristics and the relation of these characteristics to electrochemical processes at the β''-alumina interface and sodium flow characteristics.

EXPERIMENTAL:

Samples:

The samples were prepared with a high rate DC magnetron sputtering apparatus (SFI model 1). The sample set consisted of four electrodes deposited on a 1.5 cm diameter β''-alumina tube with nominal wall thickness of 1 mm. These four electrodes were used for electrochemical measurements while a duplicate set of samples was deposited on polished single crystal sapphire substrates for microscopic examination and chemical analysis. The

tube electrodes and duplicate samples were deposited simultaneously with the substrates equidistant from the sputtering target to insure identical deposition conditions. The four electrode compositions were:

1. Pure molybdenum, the present electrode of choice, to serve as a bench mark for comparison.
2. Mo-Ti alloy of low Ti content, nominally ~1%.
3. Mo-Ti alloy of high Ti content, nominally ~3%.
4. LaB_6

All electrodes were between 1.5 and 2.0 μm thick.

Measurements:

Measurements were made on the test electrodes and duplicate sample electrodes to determine the electrochemical performance under simulated AMTEC operating conditions, to determine the changes in performance with time under these conditions and to relate the performance and performance changes to the morphology and compositions of the test electrodes. These measurements consisted of:

1. Voltage-current curves of each electrode on the β''-alumina tube at 600, 700, 800, and 900 C. The electrodes were kept at 800 C for 53 hr and at 900 C for 113 hr with voltage-current measurements made at intervals to measure the rates of change of the electrochemical parameters.

2. Transient electrochemical measurements were made on each of the test electrodes at intervals during the test periods at 800 and 900 C.

These measurements consisted of establishing a steady state current in an electrode and then interrupting this steady state with a fast FET switch. The rationale of this meaurement is that immediately after the switch opens all of the ohmic voltage drops in the cell, which are due to the flow of current, vanish and the difference between the voltage at this instant and at open circuit is due to sodium flow polarization.

The voltage V_+ measured immediately after the current is interrupted is given by,

$$V_+ = (RT/F)\ \ln(P_2/P_4). \qquad (1)$$

where P_2 and P_4 are the effective sodium pressures (activities) at the interfaces shown in Fig. 1, T is the temperature of the electrode, R is the gas constant and F the Faraday. The Na pressure at the solid electrolyte - porous electrode interface is,

$$P_4 = P_3 + P_{43} \qquad (2)$$

P_{43} is the pressure drop through the porous electrode. P_3 is the evaporative pressure necessary to cause transport of Na vapor to the condenser surface at a rate equal to the steady state electrochemical production of Na by the current density i, plus a small term δ due to evaporation of Na vapor from the condenser. The evaporative pressure resulting from current density i existing before current interruption is found from the kinetic theory of gases to be $(2\pi MRT)^{1/2}i/F$, thus

$$P_3 = (2\pi MRT)^{1/2}i/F + \delta = Xi + \delta \qquad (3)$$

When i is more than ~0.01 A/cm^2 the term δ can be neglected. Since all of the quantities on the right hand side of Eq. (3) and P_2 are known, a value of V_+ can be calculated for an ideal electrode with $P_{43} = 0$. Denoting this by V_+' we have,

$$V_+' = (RT/F)\ln(P_2/Xi) \qquad (4)$$

Substituting Eq. (2) in Eq. (1) and subtracting Eq. (1) from Eq. (3) we find the flow resistance polarization voltage,

$$\Delta V = V_+' - V_+ = (RT/F)\ln[(Xi + P_{43})/Xi] \qquad (5)$$

Thus the difference ΔV between theoretical and experimental current interrupt voltages gives the ratio of pressure at the solid electrolyte - electrode interface (P_4) to the pressure at the porous electrode-vacuum interface (P_3) independent of resistive voltage drops in the solid electrolyte porous electrode

or test leads.

3. Resistivity measurements on the duplicate electrode samples in the as-deposited condition and after vacuum annealing at 1000 C to simulate AMTEC operation.

4. Scanning electron micrographs of the duplicate electrode samples in the as-deposited state and after vacuum annealing for 8 hr at 1000 C. The polished sapphire substrates were required for these experiments because the surface roughness of the β''-alumina tube was greater than the electrode thickness, making measurement of the film thickness uncertain.

5. Secondary ion mass spectrometric analysis of the duplicate samples in the as-deposited and vacuum annealed states.

6. Atomic absorption analysis of the duplicate samples was performed by Galbraith Laboratories.

7. Differential thermal analysis and X-ray diffraction measurements were made on the LaB_6 to confirm the amorphous (glassy) morphology of these films and to determine the amorphous to crystalline transition temperature.

RESULTS:

The steady state electrochemical measurements showed voltage -current density curves fitting the mathematical form V = A - Bln(i + k) - iR. This is the form of the voltage - current density curves that has been derived theoretically for the AMTEC. Measured voltage - current density curves fell below those calculated for an ideal electrode (i.e. an electrode having no sodium flow resistance and no electrical sheet resistance). The parameter A, which is a function of the sodium flow resistance of the porous electrode, was less than calculated for an ideal electrode and showed further decrease with time at elevated temperature while R was larger than the ideal value and increased with time at high temperature. Typical voltage - current curves are given in Fig. 2 along with osciloscope traces showing voltage jumps observed when the current is interrupted.

The independent resistivity measurements of the as-deposited electrodes were found to be 37, 50 and 90 μΩ cm for the Mo, 1% and 3% electrodes respectively. After 1000 C vacuum annealing the resistivities were found to be 25, 46 and 100 μΩ cm for the three metal electrodes. These resistivity changes were insufficient, by themselves, to have caused the observed changes in the V-i characteristics of the electrodes. Postmortem examination of the electrodes after completion of the tests showed that the electrical lead wires to the test electrodes had loosened due to thermal cycling during the tests. The resulting increase in contact resistance accounts for at least part of the observed increase in R. Designs for maintaining more effective contact between electrode and leads are now being developed.

Maximum specific power from the metal electrodes found at the beginning of tests were 65, 54 and 48% of the theoretical value for an ideal electrode for Mo, 1% and 3% Ti respectively when operating at 900 C. All three showed power loss with time at 900 C at approximately the same rate. This is illustrated in Fig. 3. The corresponding peak specific power densities were .85, .70 and .62 w/cm^2.

Our transient electrochemical measurements, utilizing the oscilloscope traces in Fig. 2, showed that the Na flow polarization (ΔV) in the Mo electrode was initially about 0.23 volt and the flow impedance of this electrode was independent of current density. During the 900 C test period this polarization increased monotonically to 0.36 volt, remaining independent of the current density. The 1% and 3% alloy electrodes showed initial flow polarizations at low current density of ~0.3 volt which increased with increasing current density i.e. the flow impedance was sodium flow dependent. By the end of the 900 C test period the flow polarization voltage had increased to 0.4 and 0.45 V at low current. Figs. 4 - 8 show plots of flow polarization voltage at 800 and 900 C for the three electrodes as a function of current density at several intervals during the test period. Fig. 9 shows a voltage vs. time curve obtained during one of the current interrupt measurements, the arrows indicate (1) the instant at which the fast switch opens and (2) the rapid voltage step following this event. It is the difference between the theoretical voltage and the top of this

voltage step that is the flow polarization voltage ΔV. It is interesting to note the relatively slow recovery of the cell to open circuit voltage. This voltage is proportional to the molar Gibbs free energy (chemical potential) of Na adsorbed on the porous electrode. The voltage along this curve could be used to determine the adsorption isotherm of Na on the porous electrode.

All three metal electrodes showed a fine (0.05 to 0.2 μm diameter) columnar grain structure under SEM examination with the columns normal to the plane of the electrode, as shown in Fig. 10. Intercolumnar spaces were estimated for the SEM's to be no more than 0.05 μm wide in the as deposited electrodes. Vacuum annealing at 1000 C caused marked changes in the granular morphology. These changes were marked by a breakup of the columns into short polygonal grains and general coarsening of the structure, particularly near the substrate electrode interface. Accurate data on the chemical compositions of the electrodes are not yet in hand since the data from the commercial analytical lab appears to be suspect. Additional duplicate samples were submitted but the analyses are not yet completed. SIMS analysis of the sputtered alloy films show that the Mo/Ti ratio is about 10, but the accuracy of the technique is not high enough to detrmine the composition to better than about a factor of 2.

Utilizing the transient electrochemical polarization measurments (V_+) and Eq. (5), the Na flow resistance in the Mo porous electrode was calculated. The calculation was carried out for 800 C and 1.00 A/cm² conditions to obtain P_{43} using $V_+ = 0.23$ V as discussed earlier. The results show that $P_{43} \cong 4 \times 10^{-4}$ atm and is greater than P_3 by a factor of 10. For comparison, an estimate of the pressure drop was also calculated assuming molecular (Knudsen) flow through pores of a size determined from SEM's of the duplicate sample films in the following manner. The electrode was assumed to be made of densely packed (touching) grain columns of 0.1 μm diameter in a square array. The remaining open area was divided into an equal number of pores and an effective cylindrical diameter of 0.05 μm calculated. Using this pore diameter and an electrode thickness of 1.5μm a pressure drop (P_{43}) of 4×10^{-3} atm was calculated to sustain a Knudsen flow rate equivalent to 1.0 A/cm² at 800 C.

Thus, another mechanism, such as surface diffusion must play a dominant role in sodium transport through the electrode, since our observed P_{43} is less than that required to support Knudsen flow by an order of magnitude. Note however that the alloy electrodes had considerably greater flow resistances than the Mo electrode, particularly by the end of the test period. The alloy flow resistances were more nearly equivalent to Knudsen flow resistances, however the resistances for these electrodes were dependent on current density (i.e. P_{43} is a nonlinear function of i).

It was found that LaB_6 can be sputter deposited on both amorphous and crystalline substrates. SEM and X-ray observations on this electrode showed it to be amorphous or glassy in microstructure with no visible pores. No crystalline X-ray diffraction peaks were deteted for the LaB_6 duplicate sample even after vacuum annealing at 1000 C for 24 hr. This appears to be the first time a metallic boride has been converted to the amorphous state and in addition 1000 C is higher than any previously reported crystallization temperature for a metallic glass. The LaB_6 electrode showed a sodium flow polarization of 0.8 V greater than the Mo bench mark electrode, indicating that this material is much less permeable to sodium vapor than metal alloy electrodes. The electrochemical cell represented by the LaB_6 electrode, the β''-alumina and the liquid Na, had an internal resistance ten times greater than the Mo and Mo-Ti electrodes due to the relatively high resitivity of this material (5900 $\mu\Omega$ cm).

Several interesting effects were observed for which only tentative ezpalinations can be given . Electrodes that had been at open circuit for several hours showed an increase in specific power during a short perod of time after current was again drawn from them. Also it appears that the electrochemical measurments are affected by the relative proximity to the electrode of the radiation sheild used in these experiments to insure a uniform temperature profile along the β''-alumina tube.

CONCLUSIONS:

At this time all of the conclusions from these experiments must be considered preliminary due to the small number of samples prepared and tested. With this caveat our conclusions are:

Pure Mo is still the material of choice for high output power electrodes. The addition of Ti to Mo does not appear to have markedly decreased the rate of power loss, however the problems with contact resistance noted above throw some doubt on this conclusion. Current interrupt measurements, which are free of contact resistance ohmic voltage drops, show a larger increase in ΔV for the Ti alloy electrodes than for Mo which supports the conclusion from the steady state measurements.

Both Mo and alloy electrodes show fine columnar grain structure with grain axes normal to the plane of the film. The alloy electrodes have smaller grains (estimated about a factor of two) and their morphology seems to be more stable at 1000 C in vacuum annealing experiments.

The Na flow resistance in the Mo porous electrode calculated from the current interrupt measurements is about an order of magnitude smaller in fresh electrodes than the flow resistance calculated from the Knudsen flow equation using the pore size and pore density from electrode SEM's. This is an important result and suggests that gas phase molecular flow is not the dominant transport mechanism in Mo electrodes. Surface diffusion in the pores and/or grain boundaries is an alternate flow mechanism that should be tested in future research. The alloy electrodes show flow resistance more nearly equivalent to the Knudsen flow resistance calculated from pore size and density.

LaB_6 can be sputter deposited on both amorphous and crystalline substrates as an amorphous thin film which retains its amorphous character up to a temperature of at least 1000 C. This appears to be the first time a metallic boride has been converted to the amorphous state and 1000 C is higher than any previously reported crystallization temperature for a metallic glass. This finding may have important ramifications in the field of metallic glasses. These materials are being investigated for use in high temperature corrosive environments such as jet engines.

LaB_6 is not a suitable candidate material for a monolithic electrode due primarily to its very low Na permeability and secondarily to its high electrical resistivity in the amorphous state. It may, however, be a worthwhile candidate to reexamine as a microgrid lithographic electrode due to its low work function which should promote rapid sodium ion neutralization at the electrode - β''-alumina interface.

Further work is needed to investigate these and additional candidate electrode materials including other Mo alloys and boride compositions. Identification of the microscopic mechanism for the low sodium flow resistance in Mo electrodes should also be a goal of following research.

T. Cole
C. P. Bankston
A. Thakoor
S. Khanna

15 Dec. 1982

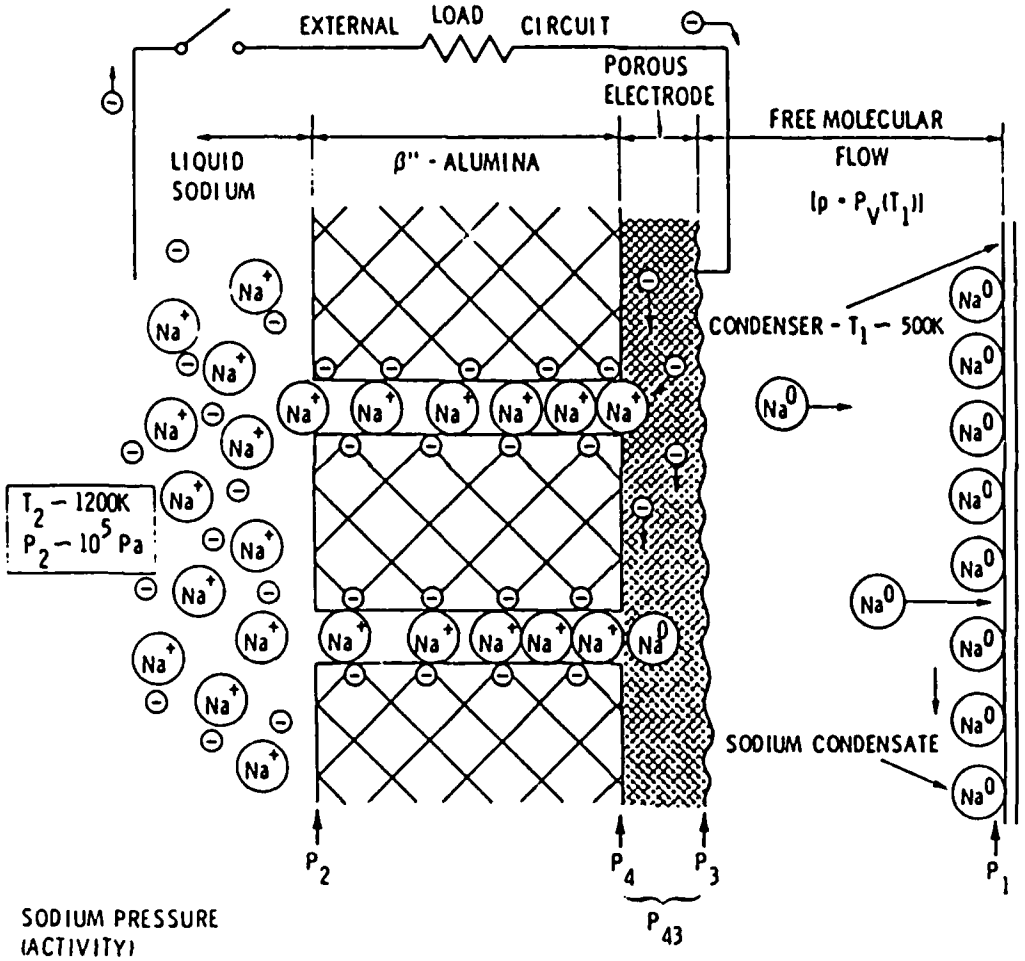

Fig. 1. Detailed Schematic of AMTEC Cycle

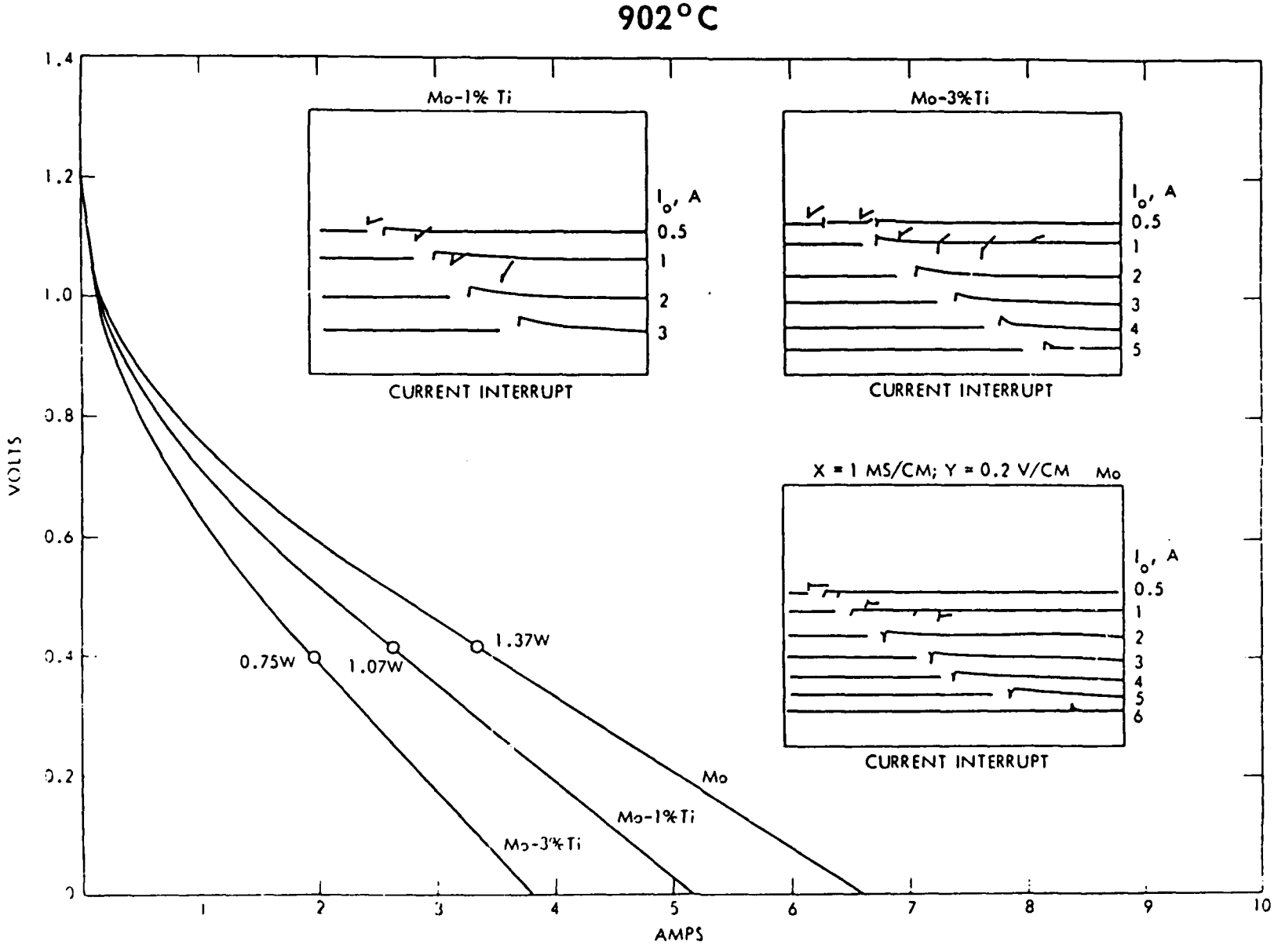

Fig. 2. Typical Current-Voltage and Current Interrupt Data

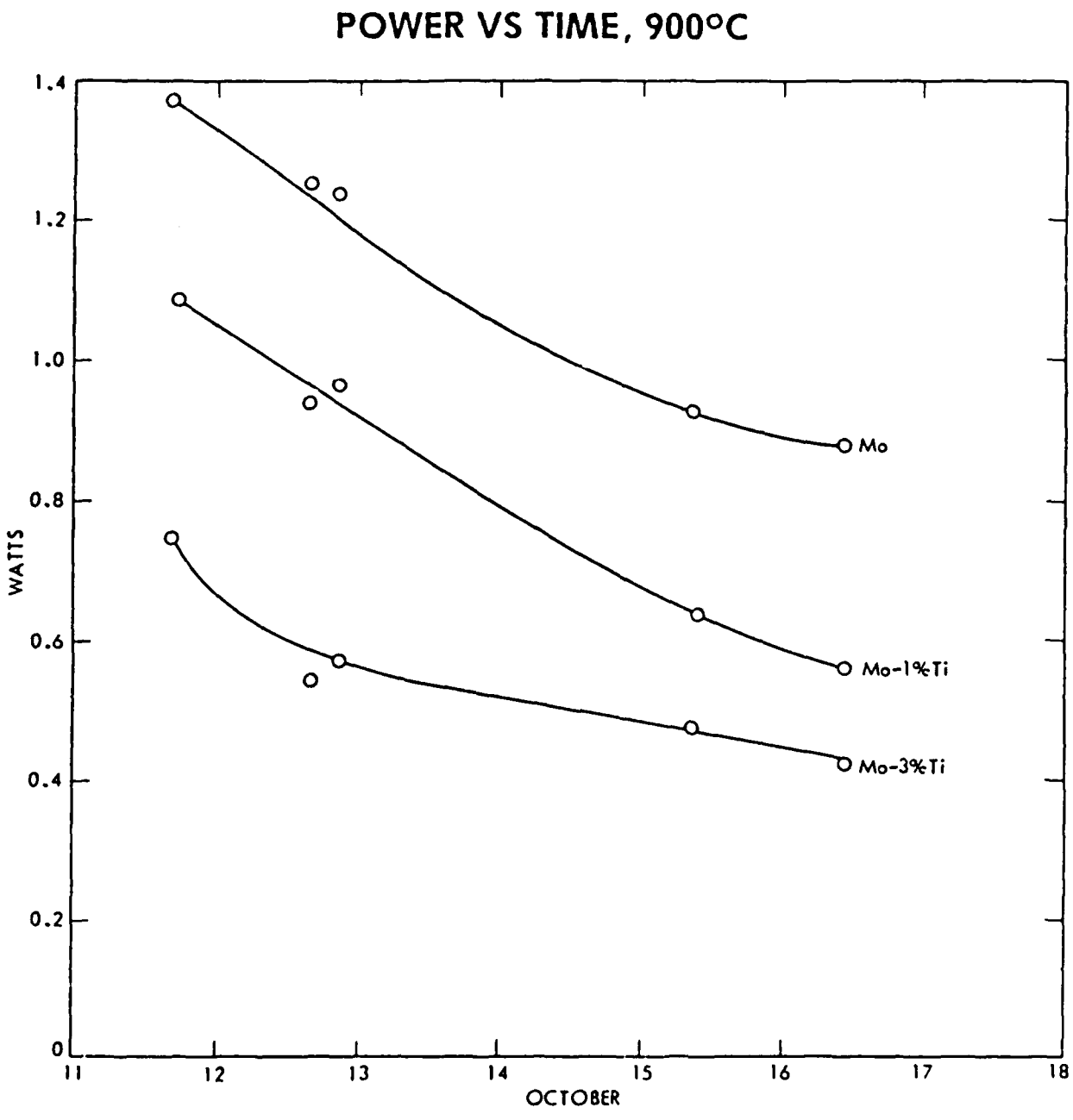
POWER VS TIME, 900°C
1.4
1.2
1.0
0.8
0.6
0.4
0.2
0
WATTS
11
12
13
14
15
16
17
18
OCTOBER
Mo
Mo-1%Ti
Mo-3%Ti

Figure 3

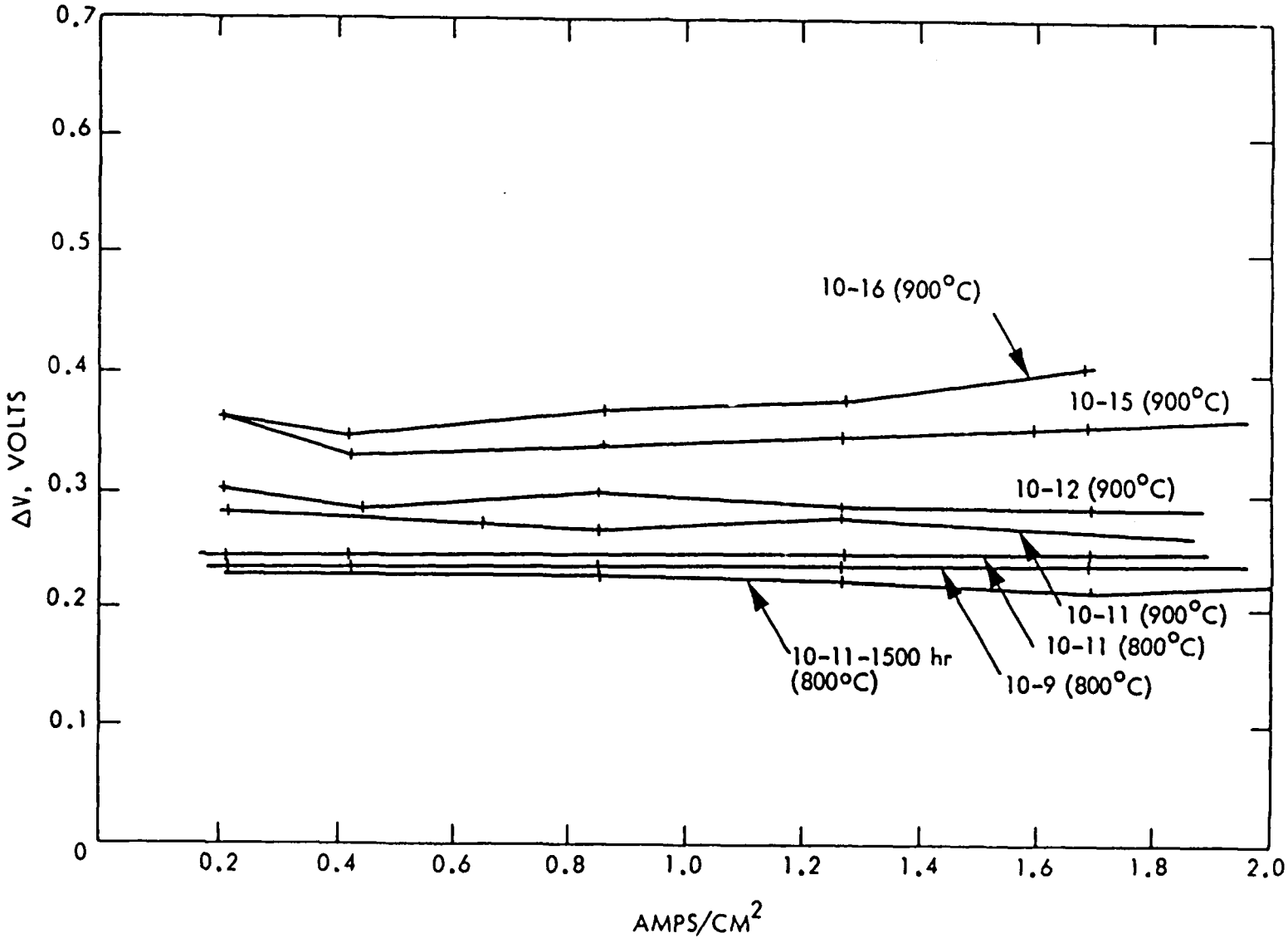
FLOW POLARIZATION VOLTAGE VS CURRENT Mo, 800°C AND 900°C
ΔV, VOLTS
0.7
0.6
0.5
0.4
0.3
0.2
0.1
0
0.2
0.4
0.6
0.8
1.0
1.2
1.4
1.6
1.8
2.0
AMPS/CM²
10-16 (900°C)
10-15 (900°C)
10-12 (900°C)
10-11 (900°C)
10-11 (800°C)
10-9 (800°C)
10-11-1500 hr
(800°C)

Figure 4

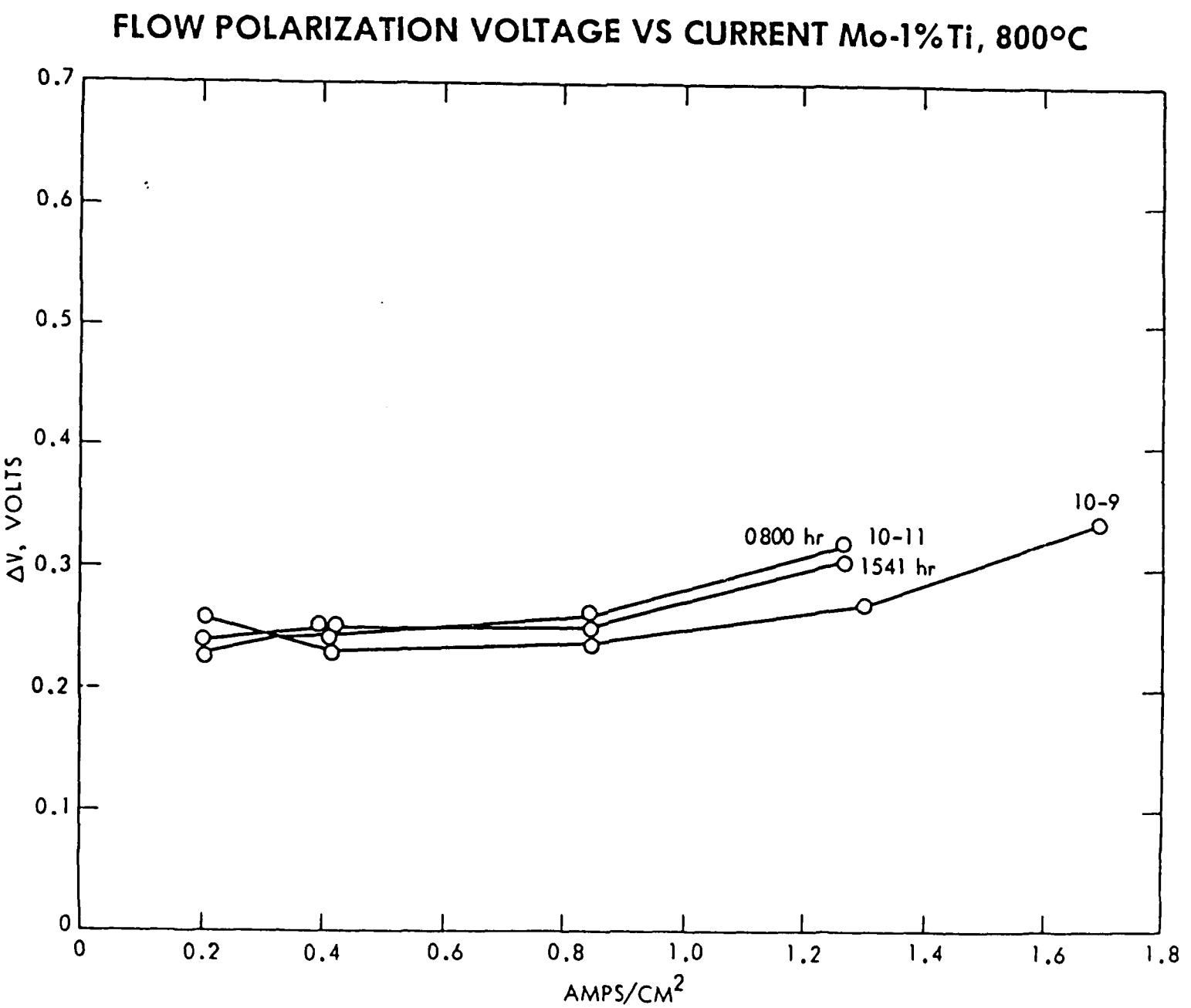
FLOW POLARIZATION VOLTAGE VS CURRENT Mo-1%Ti, 800°C
0.7
0.6
0.5
0.4
0.3
0.2
0.1
0
ΔV, VOLTS
0800 hr
10-11
1541 hr
10-9
0
0.2
0.4
0.6
0.8
1.0
1.2
1.4
1.6
1.8
AMPS/CM2

Figure 5

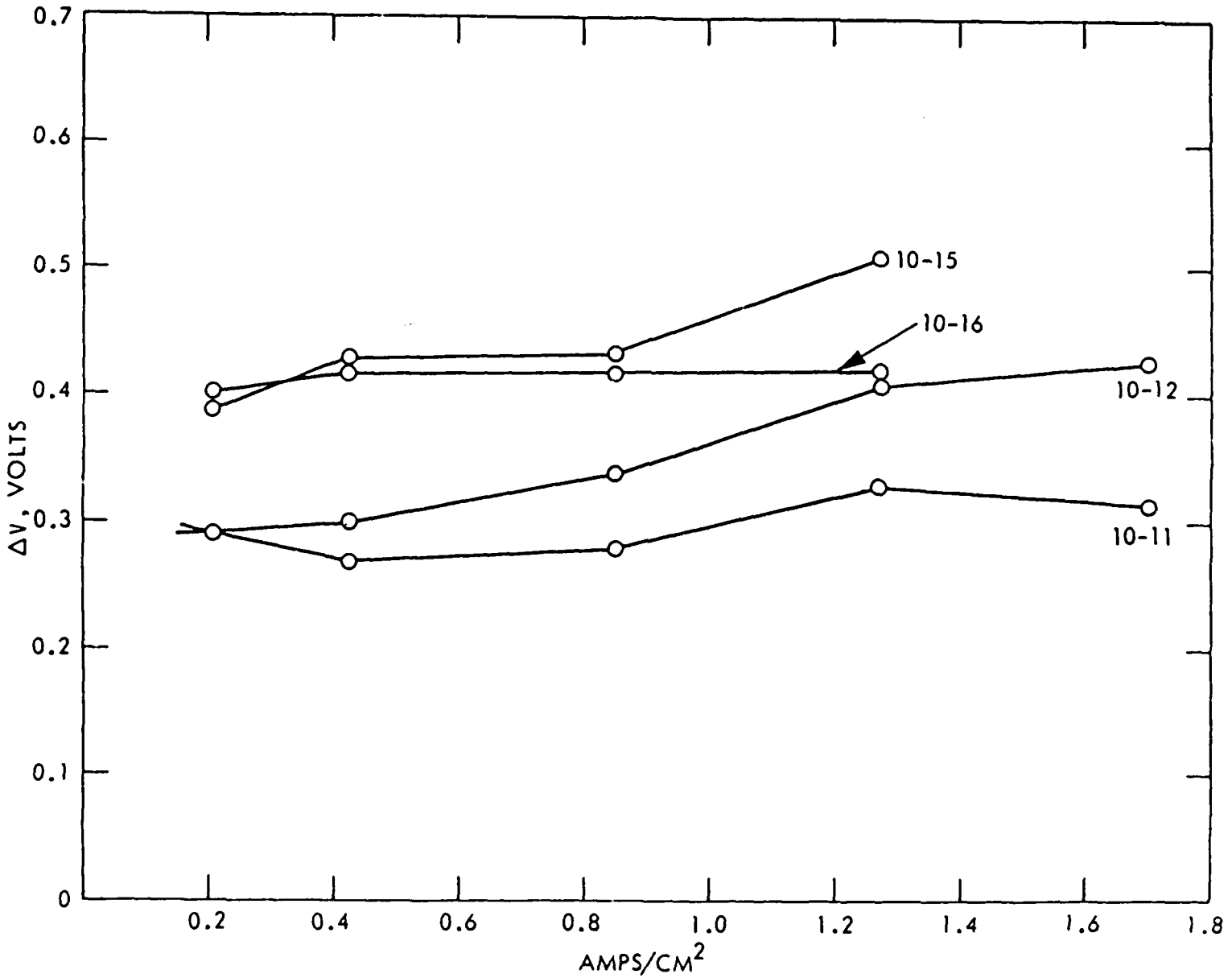
FLOW POLARIZATION VOLTAGE VS CURRENT Mo-1%Ti, 900°C
0.7
0.6
0.5
0.4
0.3
0.2
0.1
0
ΔV, VOLTS
10-15
10-16
10-12
10-11
0.2
0.4
0.6
0.8
1.0
1.2
1.4
1.6
1.8
AMPS/CM2

Figure 6

FLOW POLARIZATION VOLTAGE VS CURRENT Mo-3%Ti, 900°C

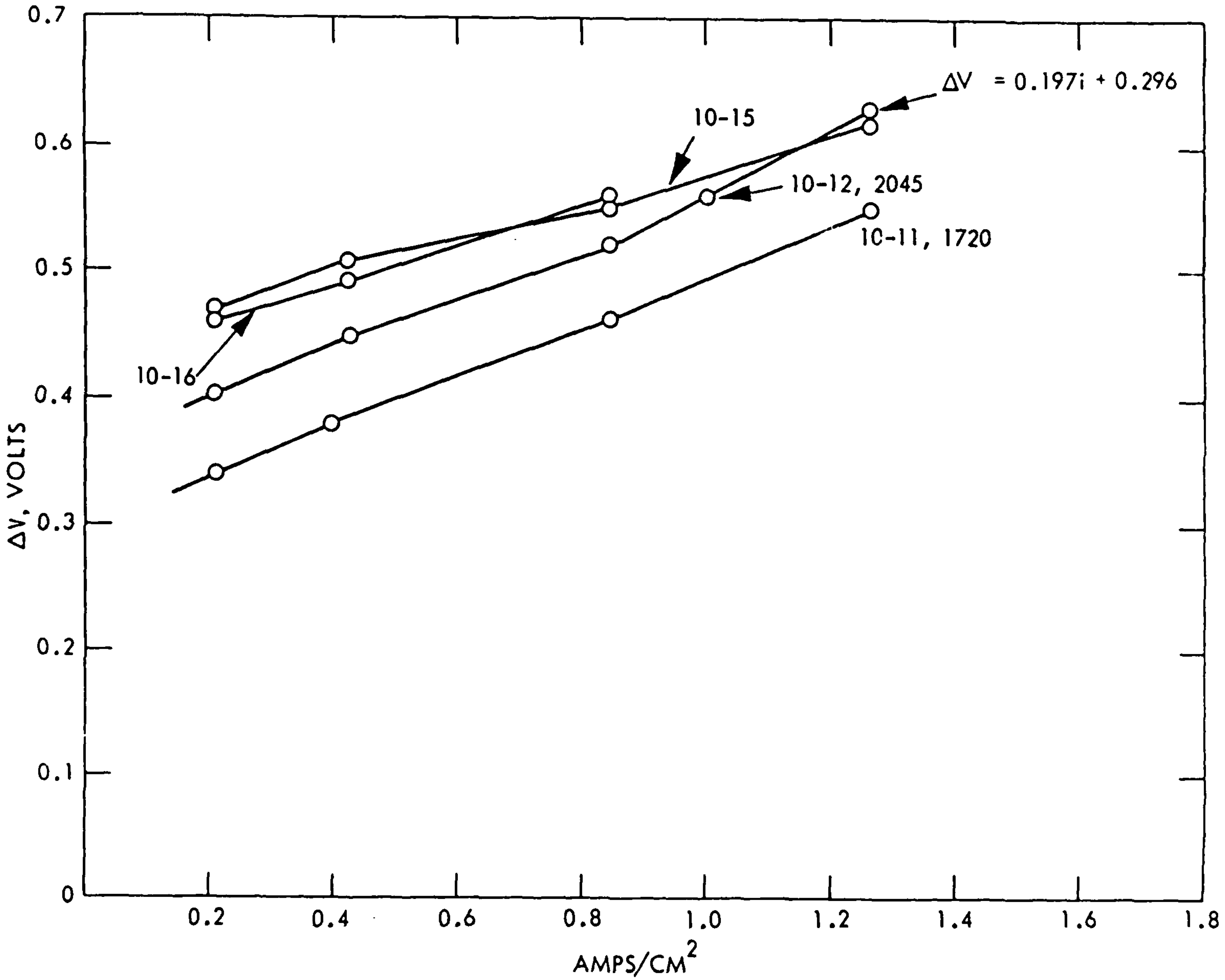

Figure 7

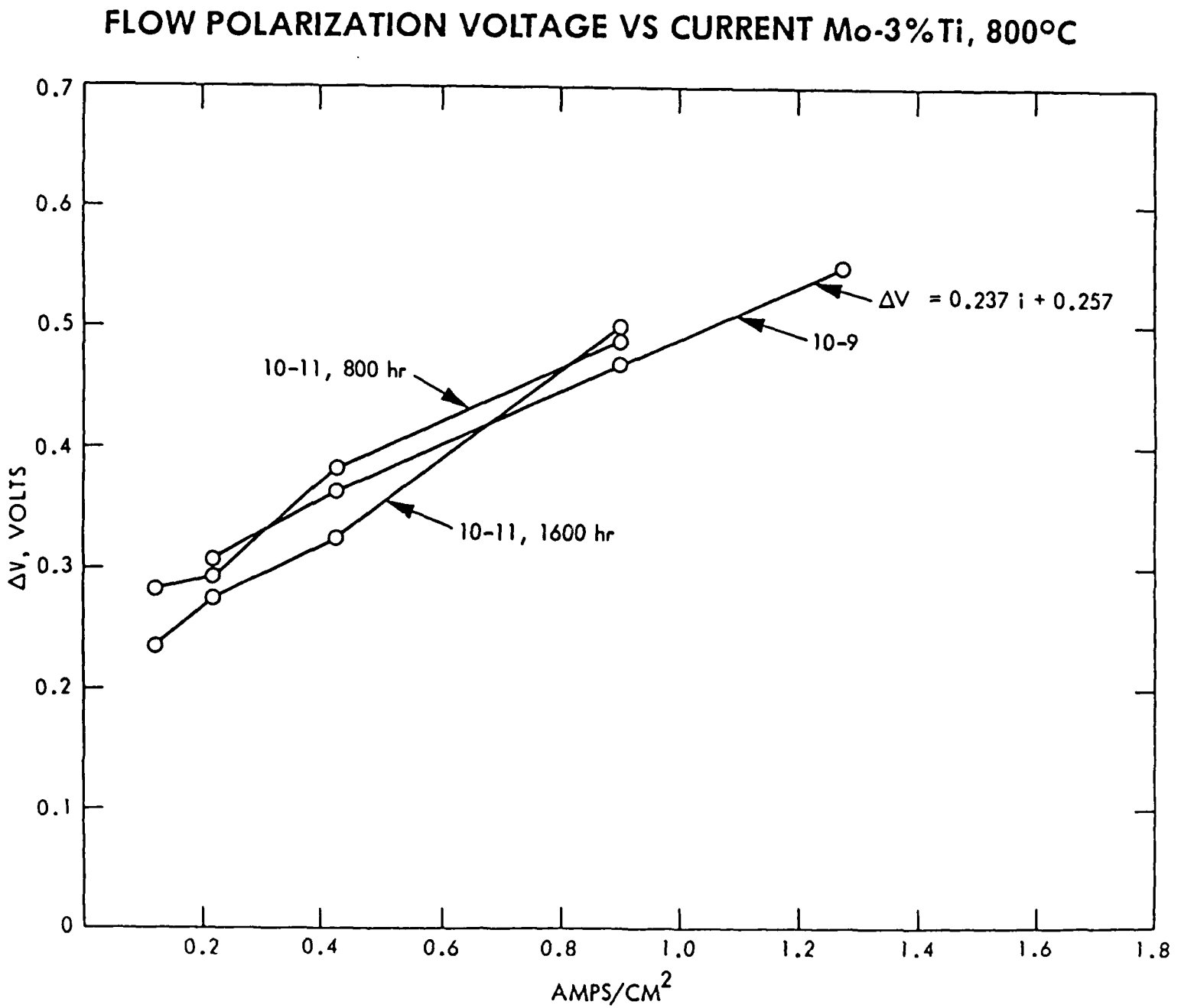
FLOW POLARIZATION VOLTAGE VS CURRENT Mo-3%Ti, 800°C
0.7
0.6
0.5
0.4
0.3
0.2
0.1
0
ΔV, VOLTS
0.2
0.4
0.6
0.8
1.0
1.2
1.4
1.6
1.8
AMPS/CM2
ΔV = 0.237 i + 0.257
10-9
10-11, 800 hr
10-11, 1600 hr

Figure 8

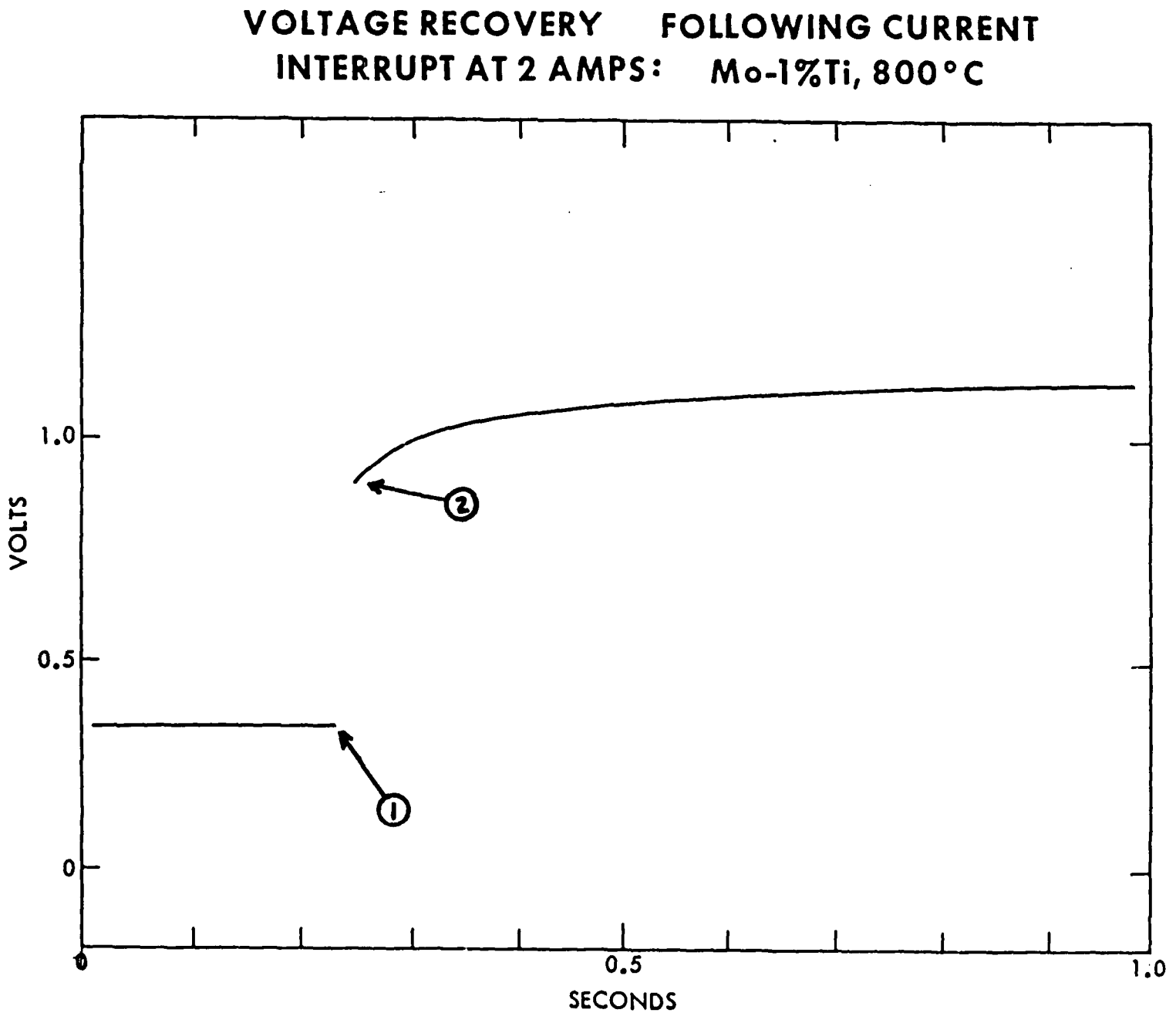
VOLTAGE RECOVERY FOLLOWING CURRENT
INTERRUPT AT 2 AMPS: Mo-1%Ti, 800°C
VOLTS
1.0
0.5
0
0
0.5
1.0
SECONDS
2
1

Figure 9

SEM OF POROUS METAL ELECTRODE FILMS SPUTTER DEPOSITED ON SAPPHIRE SUBSTRATE

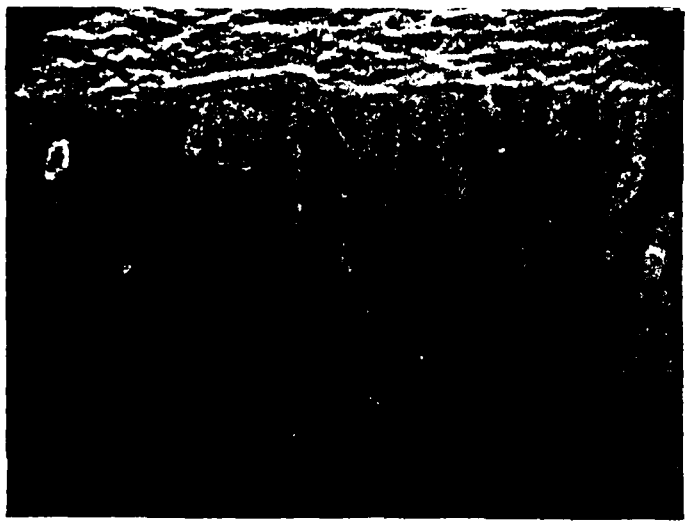

PURE Mo - AS DEPOSITED

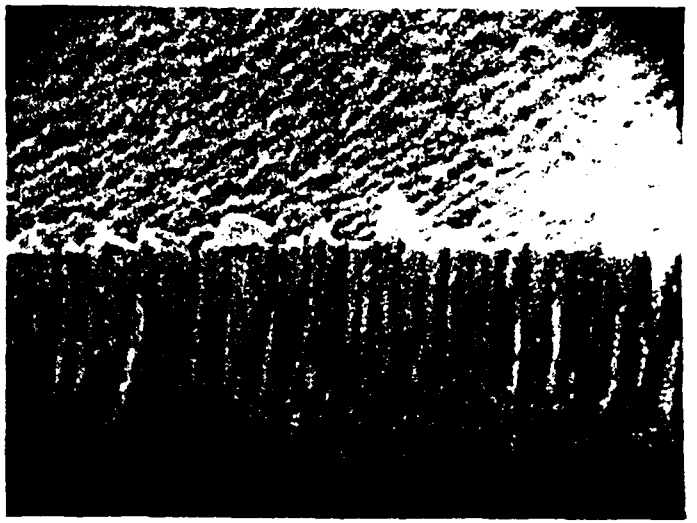

Mo - 1% Ti ALLOY (NOMINAL)
AS DEPOSITED

1 μm

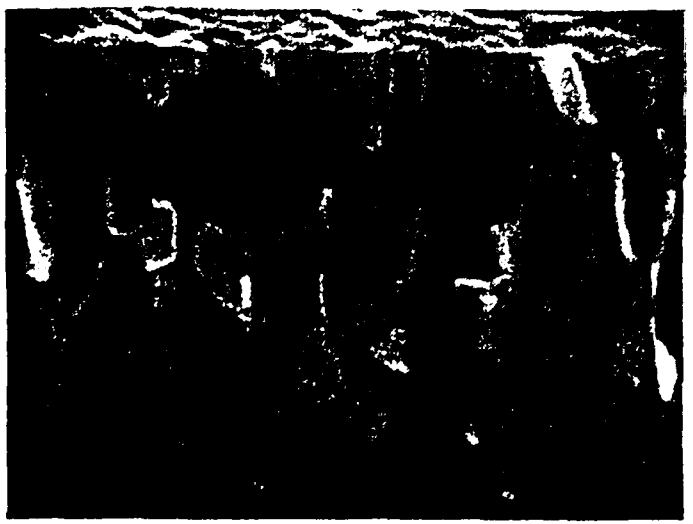

PURE Mo - ANNEALED AT
1000°C FOR 8 hr

Mo - 1% Ti ALLOY (NOMINAL)
ANNEALED AT 1000°C FOR 8 hr

Figure 10.

MPD THRUSTER EROSION RESEARCH

Final report covering the period July 1, 1982 through Dec. 31, 1982.

Statement of Work:

The tasks to be performed in the MPD thruster research were as follows:

a. Investigate the physical mechanisms inherent in plasma and arc thrusters that contribute to high erosion and provide lifetime limitations.

b. Define the methodology for both experimental and analytical investigations.

c. Initiate an experimental study on the magnetoplasmadynamic (MPD) thruster anode sheath, and fabricate and calibrate the diagnostics that will be required in an experimental investigation. These diagnostics will include electric and magnetic field probes, and an anode calorimeter. The feasibility of non-intrusive diagnostics will be considered.

PHYSICAL MECHANISMS RESPONSIBLE FOR EROSION

CATHODE

At the cathode there are four erosion mechanisms.

1) MACROSPOTS-These occur during warm-up and give rise to large loss of material due to excessive local heating. It is thought that this mechanism can be eliminated by using suitable starting techniques (low rate of current increase or auxillary pre-heating).

2) MICROSPOTS-These spots, which occur in vacuum arcs, are small regions (of the order of microns in diameter) which carry extremely high currents ($\sim 10^4$ -10^8 A/cm^2).

The key question in the MPD thruster is can a spot-free, diffuse current attachment mode exist. If so, under what conditions? The answers to these questions are initimately tied-up with the electron-emission mechanism.

3) SPUTTERING-Sputtering of the cathode will occur due to bombardment by energetic ions and neutrals.

Three sources of energetic ions/neutrals striking the cathode surface can be identified:-

i Ions Accelerated Through The Cathode Fall

ii Ions Accelerated By J x B Force

iii Charge-Exchange Neutrals

Fluxes, charge state and energy distributions of each of these categories, threshold energies, and yields at low energies and high temperatures need to be determined.

4) EVAPORATION-At high enough temperatures, the cathode will evaporate. The loss of material can be expressed by the so-called Langmuir formula:-

$$\Gamma_o = \frac{P_{ev}(T)}{4\,(m_o\,kT/3)^{1/2}} \qquad (1)$$

where $P_{ev}(T)$ is the equilibrium vapor pressure

m_o is the mass of the neutral particles

T is cathode temperature

Γ_o is the neutral particle flux.

The effects of the plasma on this rate are not known and must be understood. Key questions are 1) at what distance from the cathode surface are the neutrals first ionized? If it is outside the electric field region then there is little chance of ion trapping. 2) How does the propellant gas affect this ionization distance?

ELECTRON EMISSION MECHANISMS

Thermionic, thermionic-field, photo-emission, secondary yield by ion impact and by metastable atoms are possible electron emission mechanisms. It is important to determine which of these processes are present and to what extent since electron emission plays an important part in the overall energy balance at the cathode surface and will probably also affect current attachment (Diffuse or spot modes) and stability.

ANODE

1) SPOT FORMATION-If the current density is increased beyond a critical value then local concentrations of current or spots can occur. This can lead to vaporization and melting of the anode with a resultant high loss of material.

Exactly what the conditions (temperature, current density and thermal characteristic of the anode material) are for anode spot formation in the MPD thruster need to be determined experimentally.

2) EVAPORATION-As with the cathode, evaporative erosion rates will be governed by the Langmuir equation (equation (1)) with similar uncertainties

due to plasma effects. Since the diffuse current attachment has a negative anode voltage (plasma potential greater than the anode surface potential) then any ions formed in the anode sheath have a probability of being drawn back to the anode thus reducing the net particle loss.

INSULATORS

Erosion of insulator surfaces will occur due to the following mechanisms:

1) HEAT TRANSFER AND EVAPORATION

Heat transfer by conduction (particle bombardment) and radiation from the discharge plasma will take place. Radiative heat transfer from the cathode and anode will also occur.

A magnetic field will decrease the plasma thermal conductivity normal to the flux lines and so may tend to protect insulator surfaces parallel to the magnetic field. Evaporative losses will be given by equation (1) modified to include plasma effects.

2) SPUTTERING

Since insulator surfaces are floating they will be at a negative potential relative to the plasma potential. The floating potential, V_{IS}, will be given by

$$V_{IS} \sim \frac{kTe}{2e} \ln \left(m_i/m_e\right)$$

For argon and an electron temperature of 2eV, V_{IS} will be ~22V and so in a similar way to the cathode sputtering may be an important erosion mechanism.

METHODOLOGY

Because of the complexity of the energy processes that occur at the electrode surfaces and large uncertainties in certain key parameters, the approach needs to be primarily empirical. Nevertheless, theoretical

investigations into the plasma sheath region should proceed in parallel with the experimental work to both determine the key parameters that need to be measured and assist in the development of a model for predicting erosion rates.

There are two major problems in experimentally investigating erosion:-

1) Ground-based tests of a full-scale, megawatt, thruster is difficult.

2) The low erosion rates necessary for long lifetime may be difficult to measure.

One way of facilitating the measurement of low erosion rates would be to operate a full-scale MW thruster for a long period. However, such an approach suffers from the following drawbacks:-

a) it is both expensive and time-consuming to obtain the erosion rate for only one set of operating conditions (and for one particular thruster geometry and one propellant type)

b) the effects of a high background pressure could invalidate the results

c) it is perhaps too early in the development of steady-state MPD thrusters to allow the design of a thruster which is both long lived and high performance.

Nevertheless such testing must be done but is best postponed until one has a better understanding of the erosion mechanisms, or conducted in parallel with more fundamental studies on scaled-down thrusters. To measure erosion rates on scaled-down thrusters, some kind of scaling is required. From the point of view of erosion, it is considered that the physical parameters that should be preserved are the electrode current densities and temperatures, materials that would be used in a full-scale thruster and plasma number densities. This in itself is not straightforward since the current densities

and temperatures on a full-scale steady-state MW thruster are not yet known. Analytic calculations of how erosion scales with thruster size would be of great value.

TECHNIQUES FOR MEASURING EROSION RATES

Accurate measurements of erosion rates is made difficult by the smallness of the erosion rates, by the fact that the erosion may be highly non-uniform over the surface and may vary with time. Does exposing the thruster to atmospheric pressure, while making an erosion measurement affect subsequent erosion rates?

Methods that have already been used to measure erosion rates include weighing (mass loss) of the thruster components and quartz-crystal micro-balance (QCM) techniques. Weighing is relatively simple and reliable but no space-resolved information is obtained.

QCM methods appear to be too inaccurate to be useful and are limited to insulator surfaces and low temperatures.

A nuclear activation technique being developed at Princeton University should be extremely sensitive, offers the possibilities of space-resolved measurements on all thruster surfaces and of in-situ measurements. However, this technique may not give correct results at the cathode, if craters, deeper than the activation depth of 20 μm, arise from microspots. Additionally, it is also possible that the nuclear activation in itself may affect the erosion rate by changing the material surface properties.

Electron microscopy can be used to determine surface topography changes due to erosion. Space-resolved measurements are possible and quantitative measurements of local erosion rates should be possible but may not be very accurate.

The scanning stylus microscope is essentially an instrument for measuring surface roughness and could perhaps be used to measure erosion rates. Essentially one would take a "picture" of the surface before and after erosion and by comparing them one should be able to obtain both local erosion rates and overall mass loss.

Both conventional (Fizeau and Twyman-Green) and holographic interferometery may be applicable. Resolution can range from one hundreth to several times the wavelength of the radiation depending on the type of interferometer.

For each surface it is essential to have quantitative measurements of the erosion rates due to each of the candidate erosion mechanisms as a function of thruster operating conditions. This is made difficult by the fact that one may not have an erosion measurement technique that allows discrimination between the various mechanisms. An outline of how this might be done for each surface will now be presented.

CATHODE

Macrospots are eliminated by soft-starts or preheating. Operating conditions for microspot-free current attachment are found by observations with a high-speed camera. Evaporative losses are calculated using the Langmuir equation (an upper bound) using a surface temperature measured by optical pyrometry. Measurement of total erosion rate will yield the erosion rate due to sputtering. At operating conditions where microspots are present, erosion rates due to sputtering may be calculated by extrapolation. However, measurements of ion energy distribution and fluxes may make calculations of sputter rates possible. Measurements of total current densities at the cathode surface and cathode falls would allow calcuations of electron emission current densities, surface electric fields and relative contributions of different emission mechanisms. Total heat fluxes to the

cathode using calorimetry should also be made to allow separation of the various components in the power balance equation.

Properties of the plasma close to the cathode surface should be measured since this plasma is instrumental in determining heat fluxes, emission mechanisms and collisional trapping of eroded material. Laser interferometric and spectroscopic techniques should allow a determination of the electron and neutral densities and electron temperature.

ANODE

At the anode, erosion measurements under spot free conditions and surface temperature measurement should allow a comparison of calculated (from Langmuir equation) and measured erosion rates. Anode falls, total heat fluxes, total current densities and plasma properties need to be measured using similar techniques as for the cathode.

INSULATORS

Measurements similar to those for the cathode/anode need to be made. Using the results a comparison of the calculated and measured erosion rates should be possible.

ANODE SHEATH STUDY

Figure 1 shows a schematic of the experimental set-up that will be used to investigate the anode sheath. Electric fields in the sheath will be measured using a floating double Langmuir probe. A probe has been designed and will consist of two tungsten wire electrodes separated by ~2mm. Each electrode will be 0.25 mm diameter by 2.5 mm long and held by a drawn and tapered 2 mm diameter quartz tube.

To measure magnetic fields and current densities, minature inductive probes have been designed and constructed. Each probe consists of 120 turns

of wire wound on a 2 by 2 mm cylinder. For protection from the plasma, the probes are inserted into glass tubes with one end sealed. A shielded and twisted pair will be used to conduct the signal through a port in the vacuum tank wall. Figure 2 shows a photograph of such a probe. Probe inductance and resistance are 72 μH and 3.2 Ω respectively. The inital design of a electronic integrator based on a high performance operational amplifier (RA-909A) is underway.

Figure 3 shows a probe carriage which will be used to move the probes in two dimensions. The carriage is capable of excursions of up to 1 metre along each axis with a resolution of less than 1 mm. Stepper motors are used to drive the carriage and it is hoped to interface the system with a HP computer allowing automated probe movement and data acquisition.

Measurement of surface temperatures will be accomplished by optical pyrometry as shown in Figure (1). It is expected that the greatest uncertainty in these measurements will be due to uncertainties in the emissivity of the anode material at high temperatures. Measurements at several different wavelengths should reduce this uncertainty. At equilibrium, heat fluxes to the anode can be calculated if the dominant heat loss is by radiation. Suitable thermal isolation of the thruster should minimize conduction losses and simple thermocouple measurements can be used to estimate conduction losses (and verify the validity of their neglect in heat flux calculations).

Non-invasive techniques that were examined included high-speed photography, spectroscopy and laser interferometry. High-speed photography using an image-convector camera is a relatively straightforward technique which should yield useful qualitative information on current attachment at the anode surface. It will be particularly useful in

determining the operating conditions under which anode spots are formed. Spectroscopic methods can, in principle, be used to measure, in a space-resolved fashion, electron densities and temperatures and ion/atom temperatures and densities. In practice, these measurements can be rendered difficult or impossible by non-equilibrium plasma effects. Since the plasma in the anode sheath region of the MPD thruster is likely to be highly non-equilibrium, the development of a theoretical model for these regions will be needed to allow quantitative spectroscopic measurements. Laser interferometry, at two different wavelengths, is capable of measuring both electron densities and neutral particle densities. A literature search needs to be carried out to determine the relative contributions of the neutral particles (propellant gas and any vaporized anode material) to the overall refractivity. Other problems that may be encountered with this (and with spectroscopy) is that of optical access to interior surfaces of the anode. One way around this access problem may be to use optical fibres but the effects of phase changes due to fibre motion (for interferometry) and high temperatures must be investigated.

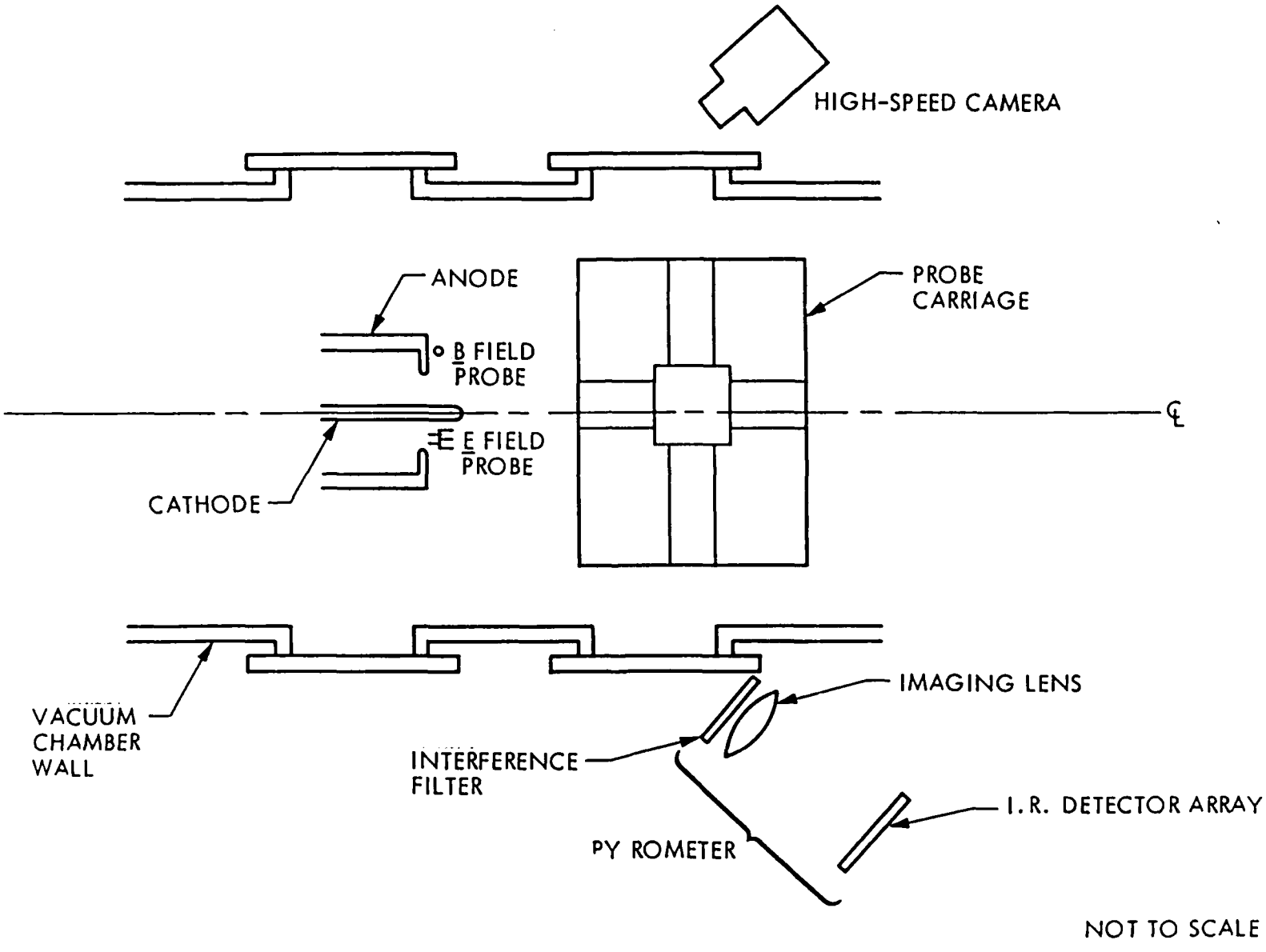

FIGURE 1. EXPERIMENTAL ARRANGEMENT

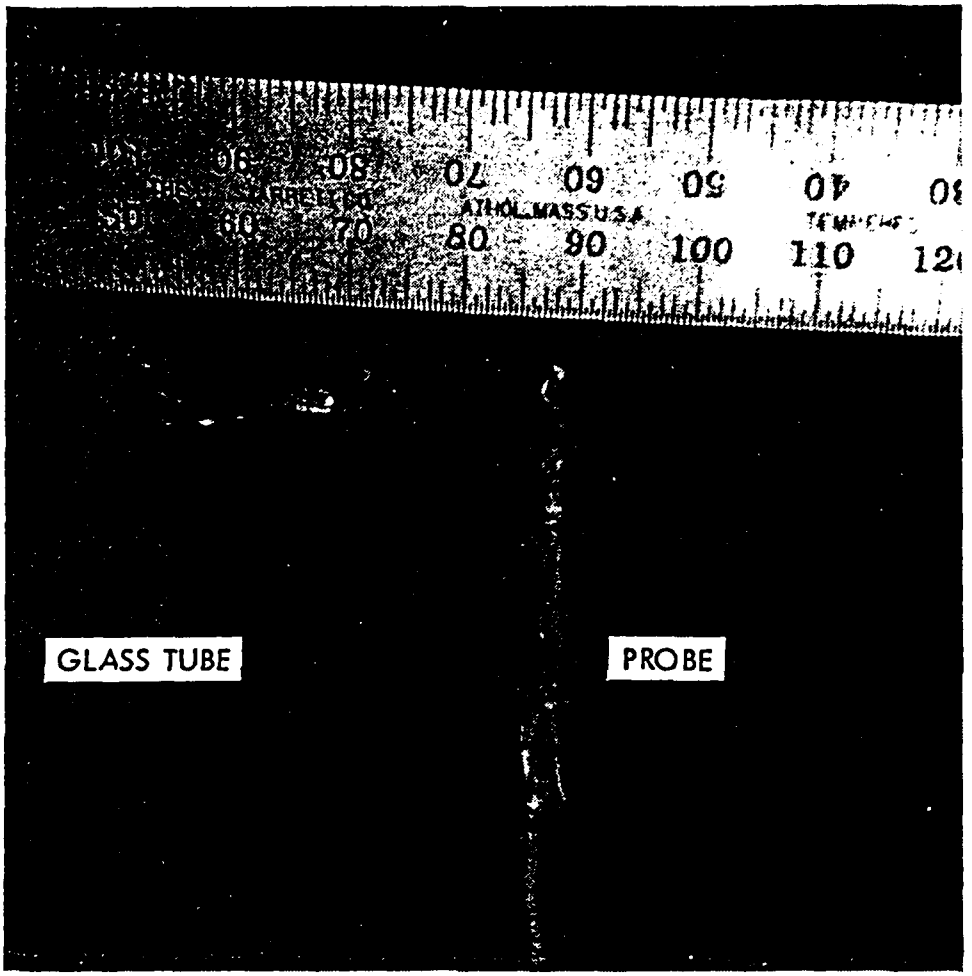

FIGURE 2. MAGNETIC FIELD PROBE

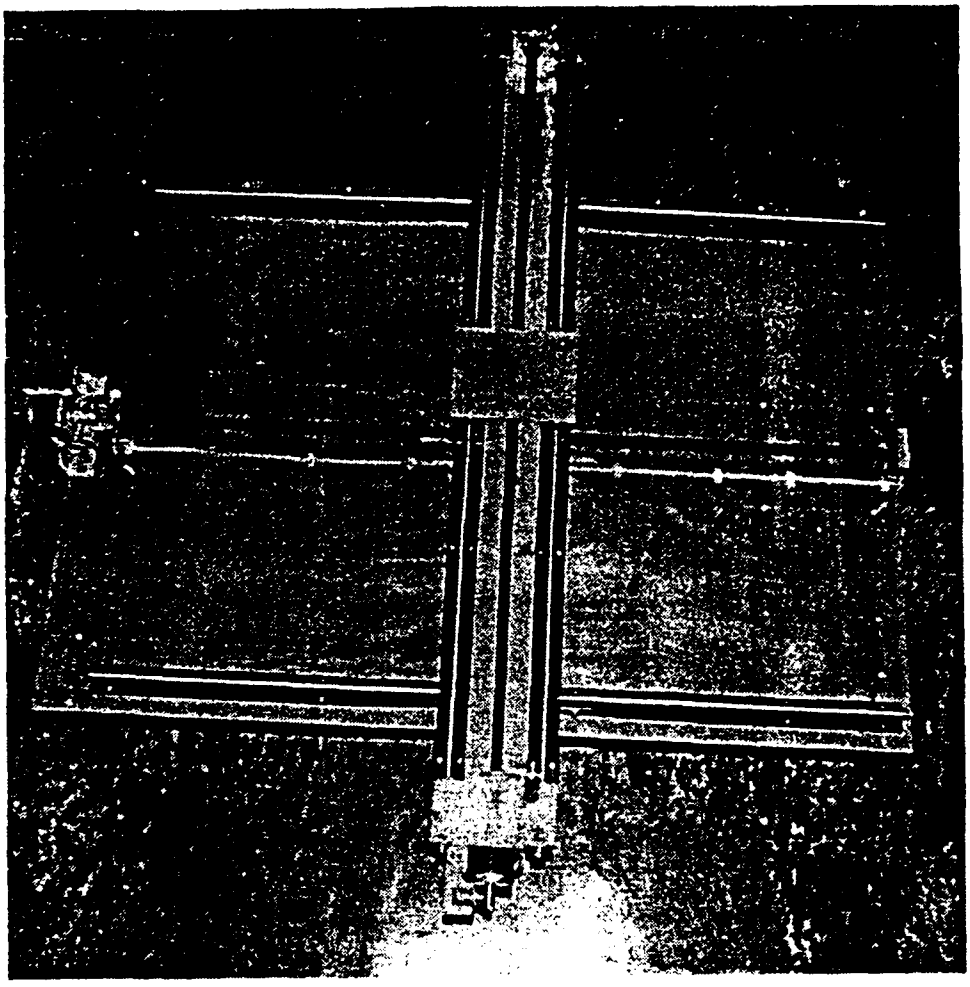

FIGURE 3. PROBE CARRIAGE

OBJECTIVE

The objective of the study was to examine and compare applicable energy conversion techniques for large nuclear space power systems. The electrical power range of the systems considered varied from 100 kilowatts to 10 megawatts. All of the conversion technologies considered should be capable of continuous electrical power generation for a time period of several years. The technologies considered, were those deemed ready for a time period of 1995 and beyond. Each of the conversion techniques was examined for limiting characteristics and an attempt was made to identify common research needs and enabling technologies.

DISCUSSION

A total of six different conversion technologies were studied in detail and compared on the basis of conversion efficiency, radiator area, overall system mass, and feasibility. Three of these systems are static conversion systems and may be made up of many small individual converters. The other three conversion technologies are heat engines which involve dynamic components. In addition, to these six, several other conversion techniques were examined in a cursory manner.

Thermoelectric conversion was the first technology examined in detail. Thermoelectric conversion has considerable space flight experience through its use in radioisotope thermoelectric generators. The limitations on thermoelectric conversion efficiency involve the material figure of merit and maximum hot side temperature. Currently, the best thermoelectric material, with flight experience, is an alloy of silicon and germanium. It has a maximum ten year lifetime operating temperature of 1280 kelvin with an average figure of merit of $0.7 \times 10^{-3} K^{-1}$. A development goal has been made to demonstrate a thermoelectric material with an average figure of merit of $1.4 \times 10^{-3} K^{-1}$ capable of long term operation at temperatures in excess of 1500 kelvin.

Thermionic conversion was the second technology examined. It is a well established conversion technique with its capability demonstrated, in the laboratory, through continuous stable high temperature operation for a period of over five years. There are two principle limitations on thermionic conversion, the first is that a high temperature heat source is required. An emitter temperature of between 1750 and 2000 kelvin is necessary for effective thermionic conversion. The other major limitation is the arc drop associated with the cesium plasma in the interelectrode gap to neutralize the electron space charge barrier. Considerable effort has gone into reducing the arc drop with only minimal progress recently. It appears that an advanced converter capable of sustained operation at 2000 kelvin with an arc drop of 0.4eV is possible.

The Alkali Metal Thermoelectric Converter (AMTEC) was the third static conversion technology which was examined. AMTEC has been successfully demonstrated in the laboratory, however, no long term stable operation performance tests have been accomplished. A self-contained recirculating AMTEC device with a thermal to electric conversion efficiency of 19% has been measured in the laboratory. The major obstacle to successful use of an AMTEC device is that when operated continuously over long periods of time the porosity of the electrode decreases due to sintering, resulting in a decrease in electrical power output. The maximum demonstrated high power electrode lifetime is only 1000 hours. Two other areas of development for AMTEC are minimizing heat losses and developing a reliable zero gravity sodium recirculation loop. Also, the maximum hot side temperature AMTEC is capable of operating at is 1400 kelvin, above this temperature the β"-alumina loses its structural integrity. The concept considered, assumed a converter capable of long life operation at 1400 kelvin with a highly reflective condensor surface to minimize radiation losses.

The Brayton engine was the first dynamic heat engine examined in detail. An inert gas closed cycle system using a single stage radial turbine and compressor with foil-type gas bearings is the Brayton engine most applicable for space power use. A variety of gas turbine space power systems have been designed and tested over the past twenty years to help identify the potential performance for these systems. In addition, continued research is under way at developing high temperature turbines for use in aircraft and other terrestrial applications. The limits to Brayton cycle conversion performance depends on the extension of turbine blade materials to higher temperatures to improve the cycle efficiency and allow for reduced radiator size. In the near term it is expected that maximum turbine blade temperatures of 1500 kelvin will be made available using molybdenum, niobium, or tantalum alloys. An advanced system should be capable of operation at 1600 kelvin through the use of ceramic turbine blades. One major difficulty with the Brayton cycle is that conversion efficiency drops off rapidly with increasing compressor temperature and therefore large radiators are needed. Also, it will be necessary to utilize multiple units to ensure reliability and assist in partial power operation.

Rankine cycles have also been designed, build, and tested for space operation. These have utilized organic working fluids, mercury, and alkali metals. Potassium is considered best for use in a high power system using a nuclear reactor heat source, unfortunately only component tests have been conducted with potassium.

The Rankine system analyzed uses a multistage axial turbine with condensate removal. It is expected that a Rankine system capable of operation at 1400 kelvin could be developed with the possibility of an advanced system capable of continuous operation at 1500 kelvin. The limits to Rankine cycle development are the maximum turbine and system temperatures and pressures which may be tolerated using a potassium working fluid. Also, in order to ensure reasonable efficiencies a complicated system with condensate removal or reheats and feedheaters is required. Similar to the Brayton cycle, it will also be necessary to use multiple units to ensure reliability and partial power operation.

The last dynamic conversion technique considered is the free piston Stirling engine with a linear alternator. The piston does not touch the wall of the expansion chamber but would be magnetically or gas dynamically suspended. The linear alternator employs a stationary coil within which the piston reciprocates with a permanent magnet. The free piston Stirling engine must be considered an advanced technology requiring extensive development before it will be applicable as a space power system. However, it is projected that an overall conversion efficiency of between 30 and 40% may be obtained. Furthermore, the Stirling engine efficiency does not drop off as rapidly as the Brayton cycle as the heat rejection temperature is increased.

Finally, several other conversion concepts were looked at but not examined in detail. The most relevant of these appears to be thermophotovoltaic conversion, which utilizes photovoltaic cells around a high temperature infrared heat source.

This technique is still in the laboratory stage, however a conversion efficiency of up to 30% has been measured. The primary limiting factor for thermophotovoltaics are that a high source temperature (~2000K) and a low cell temperature (~500K) are needed for efficient operation. MHD was also examined briefly. It appears to become reasonable only at electrical power levels in excess of 10 megawatts. So far, only minimal research work has been performed on steady-state closed cycle MHD systems. Pyroelectric conversion was also looked at. Only low temperature, low power, low efficiency devices have been demonstrated in the laboratory. Generally, pyroelectric conversion does not appear to be viable for a large space power system.

RESULTS

Table 1 contains a range of system masses, sizes, efficiencies, and operating temperatures for each of the conversion techniques at an output 1 megawatt of electrical power. The final report will contain a detailed description of the analyses and results for each of the technologies over an electrical power range from 100 kilowatts to 10 megawatts.

From the table, the two conversion types which appear the best are AMTEC and the Stirling engine. However, these two are the most speculative and are still in the early laboratory development phase. Also, it is usually recognized that studies based on early laboratory data tend to overestimate performance and underestimate total masses. Thermionic conversion appears attractive if a high temperature reactor is developed. Thermoelectric conversion appears to

be the least desirable for a high power far term system. Brayton and Rankine cycles have similar performance depending on the requirements, but the Brayton cycle is simpler and should have less development problems.

CONCLUSIONS

No one conversion type appears to be best for all requirements. The choice of a specific conversion type should depend quite strongly on the specific mission requirements.

There are several important areas which need development for a large nuclear space power system. The first of these is the development of a multimegawatt high temperature nuclear reactor. Another area of development, particularly for the dynamic conversion systems, is the need for high temperature materials. Also, particularly for systems with electrical power levels greater than 1 megawatt, it is important to develop a lightweight radiator. Specifically, the concept of a liquid droplet radiator appears to be particularly promising.

The concept of using a combination of two conversion techniques, appears to warrant some additional study. A particularly attractive combined system would appear to be thermionic conversion combined with AMTEC. Both can be used as small modular converters and have the potential for a very high combined efficiency. These two match up particularly well, because thermionic conversion is a high temperature technique, whereas AMTEC is limited to moderate temperatures. Another combined cycle which appears promising for electrical power levels greater than 10 megawatts is the combination of MHD with Brayton. Both are large scale power systems which could utilize the same working gas and offers the possibility of very high conversion efficiencies and power levels over a broad temperature range.

TABLE 1. 1 MEGAWATT ELECTRICAL POWER SYSTEMS

CONVERSION TYPE	TECHNOLOGY READINESS	HOT SIDE TEMPERATURE (Kelvin)	OVERALL SYSTEM EFFICIENCY (Percent)	RADIATOR AREA (M^2)	TOTAL MASS (Kilograms)
Thermoelectric	Best	1350 - 1500	7 - 12	600 - 1100	10,500 - 17,000
Thermionic	Good	1750 - 2000	11 - 16	130 - 190	7,000 - 9,100
AMTEC	Lab	1250 - 1400	14 - 24	300 - 570	6,400 - 10,300
Brayton	Good	1500 - 1600	34 - 37	700 - 800	8,900 - 9,500
Rankine	O.K.	1400 - 1500	19 - 21	200 - 240	9,100 - 9,600
Stirling*	Lab	1500	30	190	6,800

*Only 1 system was sized based on preliminary data